Integrated In Vitro and In Silico Approaches for Hydrogel-Based Dye Adsorption: Synthesis, Characterization, and Implementation of a Novel 3D-Printed Wastewater Filtration System

Catherine Chen, USA

Entry to the Stockholm Junior Water Prize (2025)

Abstract

The textile industry has more than doubled from 2020 to 2024, disrupting ecosystems. Current remediation methods like coagulation-flocculation are energy-intensive and costly. Biodegradable hydrogels, with hydrophilic functional groups and porous structures, offer a sustainable alternative. This study optimized hydrogel-based dye remediation of Methylene blue (MB) and Methyl Orange (MO) using computational and experimental approaches. To predict the hydrogel-dye interactions at a molecular level, computational simulations (Avogadro, Auto Dock Vina, ORCA) screened 30 hydrogels based on their binding energies, identifying four promising hydrogels (beaded, emulsion templating, dual crosslinking, and CH/GG/CR). They were tested for physical properties, dye adsorption, dye desorption/reusability, surface charges, temperature stability, functional groups, and biotoxicity. A novel self-cleaning 3D-printed column was developed to enhance dye adsorption efficiency by minimizing clogging and enabling continuous operation with minimal human intervention. Statistical analysis was conducted using a one-way analysis of variance (ANOVA), followed by Tukey's post hoc. The CH/GG/CR hydrogel achieved the highest efficiency($p<0.05$), reducing MB and MO concentrations to 0.33 ppm and 0.64 ppm($p<0.05$), respectively. Graphene oxide further enhanced adsorption, achieving reductions to 0.2 ppm (MB) and 0.4 ppm (MO); however, the additive of the CQD showed the best balance of efficiency and cost effectiveness. FTIR analysis confirmed the presence of key functional groups (OH, $NH2^{-}$). Biotoxicity tests showed minimal effects. Reusability tests with HCl (MB) and NaOH (MO) were effective. This waste product is a concentrated dye solution which could be reused in industries to directly contribute to the circular water economy. Due to the material and cost constraints, some future studies should explore the scalability of these biodegradable hydrogels under varying flow rates and environmental conditions.

Table of Contents

III. Key Words

Hydrogels, dyes, functional groups, electrostatic interactions, hydrogen bonding, π–π stacking, Binding energy, point of zero change, carbon lattice, density functional theory

IV. Abbreviations and Acronyms

Chitosan, Gellan gum, K-carrageenan hydrogel (CH/GG/CR), Methylene blue(MB), Methyl orange(MO), Carbon quantum dots(CQDs), Graphene oxide (GO), Ethylene glycol (EG), Density Functional Theory(DFT), Point of zero change (PZC), thermogravimetric analysis (TGA), binding energy(BE), Dual crosslinking hydrogel (DC), Emulsion templating hydrogel (ET), Fourier Transform Infrared (FTIR), Activated carbon (AC), parts per million (PPM)

V. Acknowledgements

I acknowledge Alison Huenger, Melanie Greenwald, Marissa Alamo, and Stephanie DiPreta for their guidance and the NYU Instrumentation Facility for allowing me to use their FTIR machine.

VI. Biography

Catherine Chen is a rising senior at Manhasset High School with a passion for environmental engineering. With both parents working in the textile industry, she became aware from a young age of the environmental impact of dye pollution, motivating her to pursue sustainable solutions. She is also a National Earth Science Olympiad top 40 finalist, a double bass student at Juilliard Pre-College, and the creator of Alzheimer's Companion, an app with over 1,000 downloads designed to help children support Alzheimer's care. Catherine hopes to continue developing innovative technologies that address critical environmental challenges.

1. Introduction

Synthetic dyes are used in many industries such as textile processing, food production, and pharmaceutical, with the textile industry being the largest consumer. As of 2023, the dyes and pigment market size share were around $41.7 billion. During textile dyeing, around 10–15% of dyes are lost in the process and enter wastewater, resulting in approximately 280,000 tons of dyes being discharged annually into global water systems. Since much of the textile industry is concentrated in developing countries that lack adequate wastewater treatment infrastructure, the discharge of untreated dye effluent poses serious environmental threats.

In aquatic systems, dyes block sunlight and impair photosynthesis in phytoplankton and aquatic plants, disrupting oxygen production and contributing to hypoxia. Contaminants like methyl orange (MO), which can form carcinogenic aromatic amines, inhibit chlorophyll synthesis, and reduce photosynthetic efficiency. Dyes, particularly persistent and bioaccumulative azo compounds, have been linked to endocrine disruption, organ damage, and increased cancer risk; methylene blue (MB) specifically interferes with DNA and RNA structures (Al-Tohamy, 2022).

Conventional dye remediation methods like coagulation-flocculation aggregate dye particles using salts such as aluminum or iron but generate sludge and secondary pollutants that require further treatment (Bahrodin, 2021). These systems are costly and less effective at low dye concentrations. Advanced oxidation processes (AOPs) demand high energy or chemical input, operate under narrow conditions, and may form toxic byproducts. Membrane filtration also requires high pressure, incurs high maintenance costs, and suffers from membrane fouling, limiting long-term use (Getya, 2023).

Hydrogels, particularly those synthesized from natural polysaccharides, offer advantages including biodegradability, high binding affinity, and ease of fabrication, making them suitable to be used in low-resource settings, without access to complex remediation techniques. Hydrogels possess a 3D polymeric structure capable of absorbing large amounts of water and capturing dye molecules through functional groups such as hydroxyl, carboxyl, and amine. These groups enable hydrogen bonding, electrostatic attraction, and van der Waals forces with dye molecules. Their reusability further enhances cost-effectiveness and sustainability (Ahmed, 2015).

Hydrogel performance can be enhanced with additives. CQDs, carbon-based nanoparticles (1–10 nm), are biocompatible and rich in surface functional groups that enable interactions with aromatic dyes like MB and increase mechanical strength and durability for long-term applications due to it being a nanofiller(Kanungo, 2023; Shabbir, 2021). Similarly, AC contributes π–π stacking via its graphitic regions and promotes ionic interactions through its oxygenated functional groups, while also enhancing porosity and thermal stability (Thamer, 2023). GO, with functional groups like –OH, –COOH, and epoxy, improves both dye uptake and mechanical strength through π-electron interactions, hydrogen bonding, and a high surface area (Guo, 2015; Liu, 2023). EG serves as a porogenic solvent, increasing pore size during synthesis to facilitate dye diffusion and absorption (Getya, 2023; Xu, 2023). Additionally, functional group modifications such as hydroxyl, carboxyl, and amine groups tune hydrophilicity, charge interactions, and crosslinking behavior. (Ribeiro, 2019; Tian, 2019; Wamba, 2018).

Given the potential for hydrogel leaching, ecotoxicity testing is essential to ensure environmental safety. Daphnia magna was selected as a model organism due to its sensitivity to pollutants, short life cycle, and ethical suitability for assessing aquatic toxicity. (Reilly, 2023).

Recent advancements in hydrogel-based dye remediation have demonstrated promising results, but certain limitations remain. Majamo et al, 2024 synthesized hydrogels from corn cob cellulose showed high adsorption capacity for MB. However, it showed instability in varying temperatures and pH levels, along with loss of efficiency upon reuse (Majamo et al, 2024).

This study aimed to simulate and identify high-performing hydrogels through computational modeling, synthesize and optimize them based on mechanical strength, swelling, and reusability, and implement them in an auto-cleaning column system for practical dye remediation. The alternate hypothesis is that in silico and in vitro-optimized hydrogels will significantly enhance adsorption efficiency and stability. This is a 6 phase approach: 1) narrow down the thousands of hydrogel candidates to the top 4 using a literature search and computational modeling simulation 2) synthesize 4 hydrogels in the lab 3) test the main hydrogels 4) add 5 additives to the best hydrogel 5) test the additive hydrogels 6) incorporate the hydrogels into an auto cleaning 3D printed column apparatus. This project addresses key gaps in hydrogel sustainability, cost-efficiency, and real-world applicability.

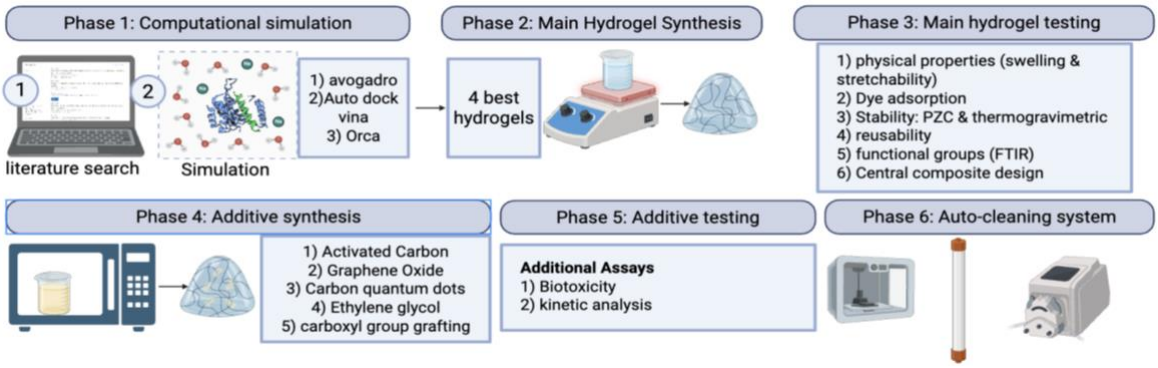

Scheme #1: Overview of the research program (created with Biorender)

2. Phase 1 *In-silico* approach

2.1 Methods - All of the below protocols were completed by the competition entrant

Initial simulations screened hydrogel structures for dye remediation based on binding energies and interactions, reducing experimental trials and minimizing waste.

2.1.1 Literature search

A systematic literature search was conducted using databases such as Google Scholar, Science Direct, and PubMed with keywords like “hydrogel”, “dye adsorption”, and “porous structure”. Peer reviewed studies from the past 10 years were reviewed to identify hydrogels with a large surface area, hydrophilic functional groups, and sustainable materials. Materials were substituted to safer alternatives to comply with school lab regulations. The hydrogels in figure 1 were the most optimal.

Hydrogels	component #1	component #2	component #3	component #4	component #5	Source
#1	agarose	citric acid				Awahiya
#2	Salep powder	montmorillonite	borax			Pourebrahim, 2024
#3	HEC	EDTA	DMAP	DMSO		Jabir, 2022
#4	gelatin	chitosan	glutaraldehyde			Ren, 2021
#5	chitosan	gellan gum	k-carreegenan			Srivastava, 2021
#6	Bentonite	Sesbania gum	acrylic acid	acrylamide	HPSI	Jiang, 2024
#7	Chitosan	Guar gum	Glyoxal			Vaid, 2023
#8	polyacrylamide	natural rubber				Martwong, 2024
#9	carboxymethyl cellul	Acrylamide	Nano-hydroxypatite			Varaprasad, 2018
#10	sodium alignate	calcium chloride	zinc chloride			cano-vincent, 2023
#11	polyvinal alcohol	sodium aligante				Hu, 2018
#12	acrylic acid	acrylamide	N,N' Methylenebisac			Sutradhar, 2024
#13	gellan gum	agarose	calcium chlroide			Ren, 2022
#14	chitosan	PVA	Glutraldehyde			Fatima, 2024
#15	Xanthan gum	chitosan	citric acid			Rahmatpour, 2024
#16	Hemicelluloses	Acrlamide	BIS	APS	TEMED	Ramirez, 2023
#17	chitosan	silica nanoparticles	tio2			Zhong, 2022
#18	sodium alignate	calcium chloride	mineral oil	pluronic F-68	tween 80	Makrygianni, 2021
#19	cellulose	CMSS	epichlorohydrin	glycerol		Tuljannah, 2024
#20	Guipi residue	Chitosan	Acylamide	Acrylic acid		Yun, 2024
#21	CMC	acrylic acid	MBD	APS		Chang, 2021
#22	chitosan	bio-hydroxypatite	genipin			Kjidaa, 2024
#23	guar gum	locust bean gum	acrylamide	MBA	APS	Kumawat, 2024
#24	chitosan	cellulose	starch	pullulan	Dextran	Stanciu, 2024
#25	Polyacrylamide	Natural rubber	MBA	APS		Martwong, 2023
#26	sodium alignate	graphene oxide	calcium chloride			An, 2024
#27	sodium alignate	acrylamide	bentonite clay	tiO2		Alijeboree, 2024
#28	chitosan	tamarind gum	calcium oxide			Rahul, 2024
#29	lignin	acrylic acid	MBA	APS		Yu, 2016
#30	Nanocellulose	Chitosan	TPP			Poornachandhra, 2023

Figure #1: List of 30 potential hydrogels and components(Figure by Competition Entrant, 2025)

2.1.2 Building the molecular structure in Avogadro: (Avogadro, 2022)

Hydrogel components were modeled and assembled in Avogadro (2022), with geometry optimized using MMFF94 for organic and UFF for inorganic parts to ensure structural accuracy. Methylene blue (MB) and methyl orange (MO) dye molecules were also constructed for interaction studies, based on literature-reported structures.

2.1.3 Molecular Docking

Molecular docking was performed using AutoDock Vina to identify ideal binding sites between hydrogels and dyes. Dyes were designated as the ligand, and hydrogels were treated as the receptor. Initial preparation in AutoDockTools remove water molecules, add Kollman charges, and add torsal tree for rotatable bonds. Hydrogel was enclosed within a grid box, and docking was executed.

2.1.4 Density Functional Theory (DFT) Analysis via ORCA (Neese, 2022)

Interaction energies between the hydrogel and the dye were calculated. Density Functional Theory (DFT) calculations were performed using the B3LYP method and def2-SVP basis set. B3LYP was chosen for its proven accuracy in predicting interaction energies in both organic and inorganic systems (Lu, 2013). def2-SVP provided the necessary polarization functions to model electron distribution in hydrogel–dye interactions. A solvent of water was defined using the SMD (Solvation Model based on Density) in the CPCM framework under ambient aqueous conditions.

2.2 Results and Discussion

Table 1: Top Four Hydrogel Systems: DFT-Calculated Binding Energies with MB and MO and Their Components

System	Components	BE (Hartree) with MB	BE (Hartree) with MO
CH/GG/CR	Chitosan, Gellan Gum, K-carrageenan	-0.05561	-0.06707
Beaded	Chitosan, Bio-hydroxyapatite, genipin	-0.06707	-0.05973
Dual crosslinking	Sodium alginate, calcium chloride, zinc chloride	-0.06567	-0.05973
Emulsion Templating	Sodium alginate, calcium chloride, mineral oil, pluronic F-68, tween 80	-0.07174	0.00781

MB = methylene blue; MO = methyl orange; BE = binding energy (Hartree)

Table #1: Summary of the top four hydrogel systems and components selected based on DFT-calculated binding energies. (Figure by Competition Entrant, 2025)

Density Functional Theory (DFT) calculations using ORCA were performed to determine the binding energies of various hydrogel systems with MB and MO in an aqueous environment. Shown in table 1, all systems exhibited negative binding energies, indicating thermodynamically favorable interactions, except for the ET + MO system(0.0078 Hartree), suggesting electrostatic repulsion due to the negatively charged COO^- groups in sodium alginate repelling the anionic MO dye. In contrast, hydrogels such as DC and beaded variants demonstrated stronger affinity for MB (–0.0657 Hartree), indicating a preference for cationic dyes (Karimzadeh, 2023).

3. Phase 2: Main Hydrogel Synthesis

3.1 Methods - All of the below protocols were completed by the competition entrant

The following subsections outline the formulation for each hydrogel. Each synthesized hydrogel was evaluated for key physical and functional properties shown in phase 3.

3.1.1 Type 1: CH/GG/CR (Srivastava, 2021)

Chitosan (1.0% w/v) was dissolved in 1.0% (v/v) acetic acid and mechanically stirred (600 rpm) overnight at room temperature to form a pale yellow viscous solution. Gellan gum (Mw = 500 kDa, 1.5% w/v) and κ-carrageenan (Mw = 788.7 Da, 1.5% w/v) were each dissolved in deionized water (90 °C) under continuous stirring(600rpm) until homogeneous viscous solutions formed. Chitosan, gellan gum, and κ-carrageenan solutions were then mixed in a 1:1:1 ratio and allowed to self-assemble into a three-dimensional polymeric network at room temperature.

3.1.2 Type 2: Beaded (Kjidaa, 2024)

A solution of chitosan (Mw = 3.8–20 kDa with a degree of deacetylation ≥ 75%) was prepared by dissolving 1g in 100 mL of 2% acetic acid. Bio-Hap (1g) was added under continuous stirring (400 rpm) for 6 hours. The mixture was dispensed using a pipet into a solution of NaOH (2% w/v) and mechanically stirred at 50 rpm for 3 hours. The obtained beads were washed with distilled water until a neutral pH was reached. The hydrogel beads were immersed in 100mL genipin solution (0.5% v/v) for 12 hours and rinsed with distilled water until a neutral pH.

3.1.3 Type 3: Emulsion Templating (Makrygianni, 2021; Kovačič, 2017)

The hydrogel was fabricated using an aqueous to oil phase ratio of 60:40 (v/v). Pluronic F-68 (0.5% w/v) was added to the hydrogel solution (99%) (350 rpm). The oil phase, mineral oil (40%) and Tween 80 (2% w/v), was premixed at 500 rpm (5 minutes) before added to the aqueous phase. The resulting solution was stirred at max speed. Polymerization was initiated by adding the cross linker under continuous stirring (300rpm). The resulting monolith was cut into 5in squares 1cm thick and soaked in ethanol for 24 hours to remove the oil, then washed with deionized water.

3.1.4 Type 4: Dual crosslinking (Cano-Vincent, 2023)

Sodium alginate (0.25 g) was dissolved in 30 mL of distilled water and stirred at 600 rpm for 1 hour at 24 °C. The solution was poured into a Petri dish, dried at room temperature for 24 hours, then at 37 °C for 48 hours to form a film. For primary crosslinking, 5 g of calcium chloride was dissolved in 500 mL of water, stirred for 15 minutes, and the dried films were immersed for 1 hour, then rinsed three times. For secondary crosslinking, films were soaked in 0.01% zinc chloride solution for 2 hours, then dried again at room temperature for 24 hours and at 37 °C for 48 hours.

4. Phase 3: Main Hydrogel

4.1 Methods - All of the below protocols were completed by the competition entrant

4.1.1 Dye absorbance assay:

4.1.1.1 Treatment with the hydrogel

Hydrogel samples were immersed in dye solutions (0.5, 1, 2, 3, and 4 ppm) for 48 hours. These concentrations were chosen based on a literature search identifying regions like Bangladesh and Cambodia where textile dye pollution contributes to water scarcity. Lower levels reflect conditions in natural water systems and allow accurate UV-Vis quantification. This also serves as a proof of concept, scaled to fit the constraints of a high school lab.

4.1.1.2 Testing using the UV-vis spectrophotometer: (Luftman, 2018)

Dye concentrations were found using a UV-Vis spectrophotometer following calibration. Measurements were performed at the maximum absorbance wavelengths: 665 nm for MB and 464 nm for MO, based on previously reported values (Wang, 2023). Dye solutions of known concentrations were prepared and measured to construct calibration curves. Absorbance values were plotted against their corresponding concentrations to generate Beer's Law plots. Linear regression analysis was used to derive the calibration equations. These equations were applied to calculate the remaining dye concentrations in the test solutions throughout the experiment.

4.1.2 Kinetic analysis: (Aljeboree, 2023)

4.1.2.1 Pseudo-first-order model

It assumes the rate of adsorption is proportional to the number of unoccupied sites on the hydrogel. The linear form of the pseudo-first order model was determined via Equation 1:

$$\ln(q_e - q_t) = \ln q_e - k_1 t \qquad \text{(Equation 1)}$$

Where Q_e is the amount of dye adsorbed at equilibrium (mg/g), Q_t is the amount of dye adsorbed at time t (mg/g), K_1 is the rate constant of the pseudo-first-order adsorption. $\ln(q_e - q_t)$ was plotted against t to obtain a straight line graph, and the slope and intercept identified $-k_1$ and $\ln q_e$, respectively.

4.1.2.2 Pseudo-second order model The pseudo second order model assumed that the adsorption rate depends on the square of the number of available adsorption sites. The linear form was determined via Equation 2.

$$\frac{t}{q_t} = \frac{1}{k_2 q_e^2} + \frac{t}{q_e} \qquad \text{(Equation 2)}$$

Where Q_t is the amount of dye adsorbed at time t (mg/g), Q_e is the amount of dye adsorbed at equilibrium (mg/g), K_2 is the pseudo second order rate constant (g/mg-min), T is time (min). t/q_t was plotted vs. t, and the slope and intercept were identified as $1/q_e$ and $1/k_2q_e$^2, respectively. k_2 was calculated via Equation 3:

$$k_2 = \frac{1}{\text{intercept} \times q_e^2} \quad \text{(Equation 3)}$$

4.1.2.3 Analysis The best model was identified by selecting the most linear plot with a r^2 value closest to 1. K, the rate constant, was quantified. The higher the k the faster the adsorption. First order may indicate a physisorption process. A second order may suggest chemisorption .

4.1.3 Desorption efficiency: (Dhahir, 2024)

Post-adsorption, hydrogels were rinsed with distilled water to remove loosely bound particles. 0.1M HCl and 0.1 M NaOH were tested. Used hydrogels (1 g) were placed into a beaker with the desorption agent (50 mL). Mixtures were mechanically stirred at 200 rpm for 2 hours. The process of adsorption and desorption was repeated until the hydrogel became unusable.

4.1.4 Physical characteristics (Ahearnee, 2012)

Swelling was evaluated by immersing 400 mg of dried hydrogel in 20 mL of deionized water for 1 hour. The swollen hydrogel was weighed, and percent weight change was calculated. Stretchability was assessed by incrementally extending the hydrogel in 2 cm intervals until rupture. The maximum elongation was recorded. Percent stretch change was calculated.

4.1.5 Thermogravimetric analysis (Reddy, 2014)

3 hydrogel samples were weighed and then heated in an oven at constant temperature (25°C, 30°C, or 35°C). At 5-minute intervals, samples were removed, cooled to room temperature, and reweighed to assess mass loss. Mass loss was plotted over time.

4.1.6 Determining the point of zero change (Dalalibera, 2020)

HCl (0.1M) and NaOH (0.1M) were used to adjust the pH of the 0.1M NaCl solution gradually while stirring the solution. The hydrogel was submerged into each pH solution and kept overnight. The final pH of the solution was measured using a pH meter. The pH at which the final pH = initial pH is the PZC. The linear interpolation was conducted in order to find the exact PZC.

$$pH_{\Delta\text{pH}=0} = pH_1 + \frac{(0 - \Delta\text{pH}_1) \cdot (pH_2 - pH_1)}{\Delta\text{pH}_2 - \Delta\text{pH}_1} \quad \text{(Equation 4)}$$

4.1.7 Toxicity Testing

Daphnia magna were cultured in natural spring water at 21 °C under a 12:12 light/dark

cycle and acclimated for 12–24 hours prior to testing. They were maintained at a ratio of 1 gallon per 100 individuals and fed daily with Chlorella vulgaris and Daphnia magna pellets. Cultures were partially refreshed weekly and maintained in triplicate to reduce population loss. (Carolina Biological) For toxicity testing, ten Daphnia magna were introduced into 100 mL of spring water containing 5 g of hydrogel. Mortality was recorded daily over the exposure period.

4.1.8 FTIR Analysis (Mohamed, 2017)

Air-dried hydrogel samples were analyzed using FTIR spectroscopy at the NYU shared instrumentation facility. Infrared radiation was passed through the samples to obtain absorption spectra, which were used to identify characteristic vibrational bands of functional groups.

4.1.9 Central Composite Design

Stat Ease was used to preform central composite design which is used to build second order models without needing to test every possible combination. It optimizes the factors of time(40-100min), initial concentration (1-4 ppm) and adsorbent dose(1-3 g/ml) to obtain the lowest final concentration. 20 possible combinations of the 3 factors were obtained and tested in the lab.

4.1.10 Statistical ANOVA:

Statistical analysis was performed using one-way ANOVA and two-way ANOVA with significance being $p<0.05$. It was run using XLMiner Analysis ToolPak.

4.2 Results and Discussion FTIR analysis confirmed the successful synthesis and functionalization of all hydrogel formulations; for example, the CH/GG/CR hydrogel showed distinct –OH, $–NH_2$, C=O, S=O, and C–O–C peaks, verifying the incorporation of chitosan, gellan gum, and κ-carrageenan.

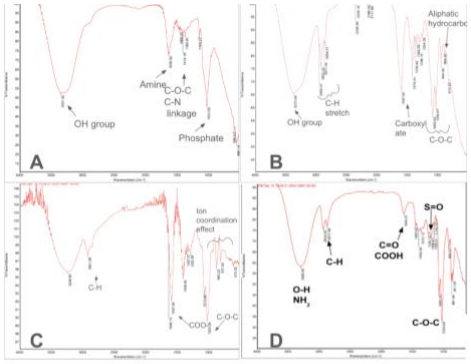

Figure #2: Fourier Transform Infrared (FTIR) spectra highlighting the presence of key functional groups, confirming the chemical structures of (A) Beaded hydrogel, (B) Emulsion-templated hydrogel, (C) Dual-crosslinked hydrogel, and (D) CH/GG/CR hydrogel. (Figure by Competition Entrant, 2025)

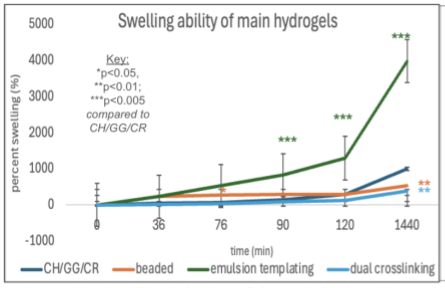

Figure #3: Swelling behavior of the main hydrogel formulations (N=3) over time after immersion in water. Data is the percent (± 1 SE). Statistical significance was determined using Anova: Two-Factor With Replication with a post-hoc Tukey Test(*p < 0.05, **p < 0.01, ***p < 0.005 compared to CH/GG/CR) (Figure by Competition Entrant, 2025)

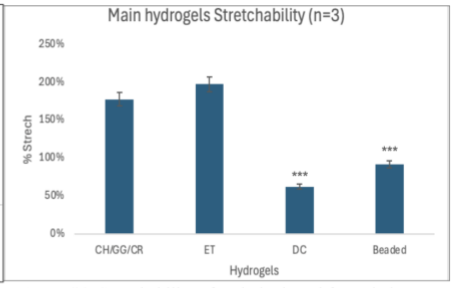

Figure #4: Stretchability of main hydrogel formulations (n=3) measured by manually stretching each hydrogel sample to determine elongation percentage. Data is the percent (± 1 SE). Statistical significance was determined using Anova: Two-Factor With Replication with a post-hoc Tukey Test(*p < 0.05, **p < 0.01, ***p < 0.005 compared to CH/GG/CR)

A one-way ANOVA revealed that the ET hydrogel demonstrated the highest

swelling capacity, exceeding 4000% after 1440 minutes ($p < 0.005$), and the highest stretchability, reaching nearly 195%. These results can be attributed to its porous, loosely cross linked structure with interconnected channels, which allow for efficient water uptake and significant deformation under tension**.** The CH/GG/CR hydrogel showed moderate swelling and high stretchability (~175%), likely due to the presence of ionic and hydrogen bonding interactions among components. The beaded hydrogel, reinforced with hydroxyapatite and crosslinked with genipin, exhibited low swelling and reduced stretchability (~90%, $p < 0.005$), reflecting its compact and reinforced internal structure. The DC hydrogel showed the lowest swelling and stretchability, consistent with its tightly packed, dual chemically crosslinked matrix that restricts both polymer expansion and deformation.

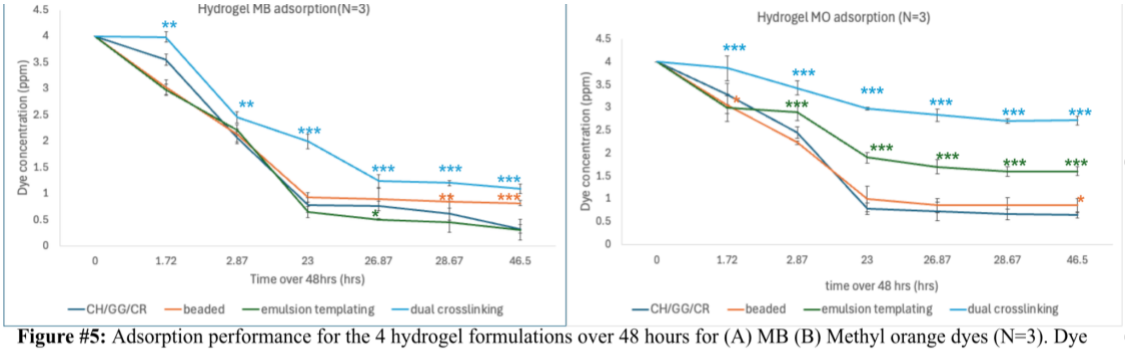

Figure #5: Adsorption performance for the 4 hydrogel formulations over 48 hours for (A) MB (B) Methyl orange dyes (N=3). Dye concentration (ppm) was measured at specific time points to assess the removal efficiency. Data is the percent (± 1 SE). Statistical significance was determined using Anova: Two-Factor With Replication with a post-hoc Tukey Test(*p < 0.05, **p < 0.01, ***p < 0.005 compared to CH/GG/CR)

In both MB and MO adsorption experiments, ET and beaded hydrogels exhibited rapid initial uptake, particularly within the first 24 hours. The ET hydrogel's high surface area-to-volume ratio and porous, interconnected structure enhanced diffusion and exposure of functional groups like COO^- and OH^-, facilitating strong electrostatic interactions with MB^+ (Lai, 2018). Although the beaded hydrogel has limited internal porosity, its spherical morphology and surface area promoted efficient early-phase adsorption (Kidaa, 2024). In contrast, dual-crosslinked (DC) hydrogels showed significantly lower adsorption for both dyes throughout the 48-hour period, likely due to their dense structure (Cano-Vicent, 2023). After 46.5 hours, the CH/GG/CR and ET hydrogels achieved high MB removal, reducing concentrations to 0.33 and 0.31 ppm, respectively, due to their anionic functional groups(COO-). However, ET showed reduced MO adsorption due to electrostatic repulsion, while the beaded hydrogel demonstrated improved MO uptake, likely due to positively charged NH_4^+ groups from chitosan. The CH/GG/CR hydrogel maintained strong

adsorption for both dyes, attributed to its diverse functional groups: NH_2 from chitosan (for MO^-), COO^- from gellan gum, and SO_3^- from κ-carrageenan (for MB^+), as confirmed by FTIR.

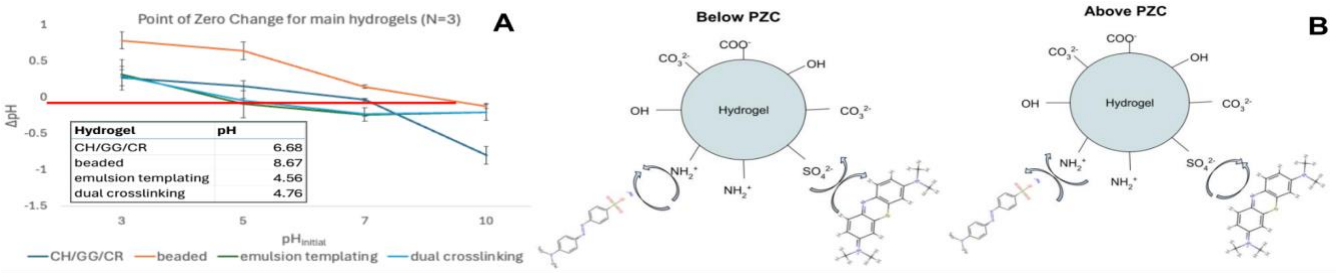

Figure #6: (A) Point of Zero Change (PZC) of the main hydrogel formulations (N=3), showing the relationship between initial pH and ΔpH after equilibration. (B) Schematic illustration of electrostatic dye-hydrogel interactions below and above the PZC.

To evaluate the pH dependent surface charge behavior of the hydrogel formulations and its influence on dye adsorption, the point of zero change (PZC) was determined using the ΔpH method. The PZC corresponds to the pH at which ΔpH equals zero, indicating that the net surface charge of the hydrogel is neutral. Surface charge polarity relative to the PZC plays a critical role in dye adsorption: below the PZC, hydrogel surfaces are protonated and positively charged (e.g., $–OH_2^+$, $–NH_3^+$), favoring electrostatic attraction with anionic dyes such as methyl orange (MO^-), whereas above the PZC, the presence of deprotonated groups (e.g., $–COO^-$, $–SO_3^-$) leads to a negatively charged surface that enhances adsorption of cationic dyes like MB^+, as illustrated in Figure 6B. (Rey, 2011) The PZC values varied across formulations shown in Figure 6A. The high PZC of the beaded hydrogel suggests a strong positive surface charge under neutral conditions, enhancing MO^- adsorption, whereas the CH/GG/CR hydrogel—with its moderate PZC and diverse functional groups (NH_2 from chitosan, COO^- from gellan gum, and SO_3^- from κ-carrageenan)—demonstrates dual functionality, capable of adsorbing both MB^+ and MO^- depending on the surrounding pH. In contrast, the consistently low PZC values of the emulsion-templated and dual-crosslinked hydrogels suggest they remain negatively charged at most environmental pH levels, limiting MO^- adsorption due to electrostatic repulsion, but favoring MB^+ binding. Furthermore, external pH modulation using HCl or NaOH can significantly impact adsorption efficiency by altering the hydrogel's surface charge. Acidic conditions (pH < PZC) induce positive surface charges, weakening MB^+ adsorption through electrostatic repulsion. Conversely, alkaline conditions (pH > PZC) promote a negatively charged surface that diminishes MO^- uptake. These findings underscore the importance of tuning both hydrogel composition and environmental pH to

optimize selective dye removal performance. Other factors such as ionic strength, temperature, and competing ions may affect surface charges and need to be considered in future studies. The data correlates to the point of zero change analysis.

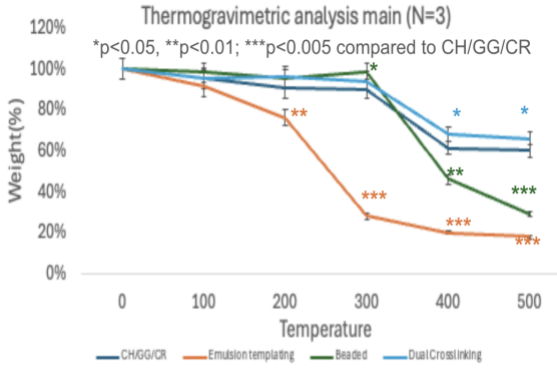

Figure #8: Thermogravimetric analysis (TGA) of the main hydrogel formulations (N=3), showing the percentage of residual weight as a function of increasing temperature. Data is the percent (± 1 SE) Statistical significance was determined using Anova: Two-Factor With Replication with a post-hoc Tukey Test(*p < 0.05, **p < 0.01, ***p < 0.005 compared to CH/GG/CR)

Figure 8 presents the thermogravimetric analysis (TGA) of the hydrogel formulations. The emulsion-templated hydrogel showed the lowest thermal stability, retaining only 20% of its mass by 500 °C due to its porous, loosely cross linked structure. While this architecture improves swelling and dye uptake, it lacks the integrity to resist thermal degradation, as the exposed labile polymer chains decompose more readily. In contrast, the dual-crosslinked hydrogel demonstrated the highest stability, maintaining over 60% of its weight at 500 °C, attributed to its dense, highly crosslinked network and thermally stable linkages. CH/GG/CR and beaded hydrogels exhibited intermediate stability; CH/GG/CR benefited from ionic and hydrogen bonding among its biopolymers, while the beaded hydrogel, reinforced with hydroxyapatite and genipin, showed improved resistance due to its compact structure. These results highlight an inverse relationship between porosity and thermal durability, underscoring the need to balance adsorption and heat resistance in hydrogel design.

The CH/GG/CR hydrogel demonstrated the best overall performance in dye adsorption, physical properties, and stability, and was therefore selected for further optimization. Seven chitosan:gellan gum:κ-carrageenan ratios were tested (1:1:1, 2:1:1, 2:2:1, 1:2:1, 1:2:2, 1:1:2, and 2:1:2), with the 1:1:1 ratio yielding the highest dye adsorption and selected for subsequent experiments.

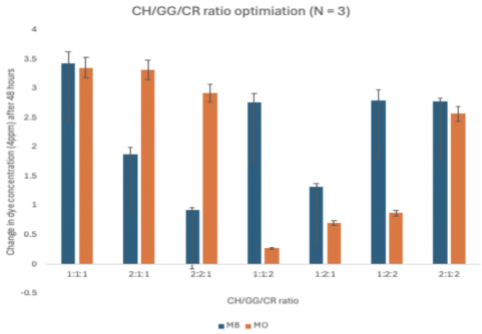

Figure #9: Optimization of CH/GG/CR hydrogel composition for dye adsorption efficiency of 48 hours (N=3). THe bar graph shows the change in dye concentration of MB and MO after treatment with hydrogels formulated at different mass ratios of chitosan(CH), gellan gum (GG), and k-carrageenan(CR). High bars indicate greater dye adsorption.

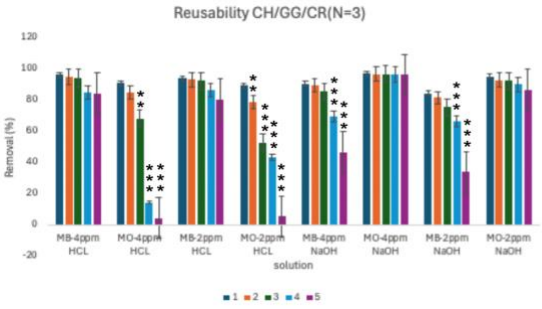

Figure #10: Reusability performance of CH/GG/CR hydrogel across five adsorption desorption cycles (N=3) for MB and methyl orange (MO) at two initial dye concentrations (2 ppm and 4ppm). Hydrogels were regenerated using either 0.1M HCl or 0.1M NaOH as desorption agents followed by reabsorption. Bars represent dye removal efficiency(%) for each cycle. Data is the percent (± 1 SE). Statistical significance determined using ANOVA: Two-Factor With Replication with a post-hoc Tukey Test(*p < 0.05, **p < 0.01, ***p < 0.005 compared to CH/GG/CR)

Figure #11: Visual comparison of dye adsorption and desorption behavior across different hydrogel formulations (A) CH/GG/CR adsorption (B) CH/GG/CR desorption (C) DC adsorption (D) DC desorption (E) emulsion templating adsorption (F) emulsion templating desorption (G)

The CH/GG/CR hydrogel was then tested for reusability with no statistically significant loss in performance after 5 cycles. HCl was effective de-adsorbing MB which is likely due to the protonation of the hydrogel's surface functional groups (COO- → COOH or NH2 → NH3+) under acidic conditions, which induces electrostatic repulsion with the cationic MB dye, promoting efficient desorption. After removal, the hydrogel rapidly re-equilibrates upon washing, retaining its capacity to rebind MB in subsequent cycles. In contrast, NaOH was more effective for regenerating the hydrogel for MO adsorption. Under alkaline conditions, functional groups such as NH3+ and SO3H are deprotonated to NH2 and SO3- respectively, enhancing electrostatic repulsion with the anionic MB causing de-adsorption. The hydrogel's ability to maintain high dye removal efficiently across cycles suggests that the ionic interactions involved are largely reversible and that the structural integrity of the hydrogel remains stable.

5. Phase 4: Additive synthesis

5.1 Methods - All of the below protocols were completed by the competition entrant

Each of the add ons was incorporated into the optimized CH/GG/CR hydrogel.

5.1.1 Creation of the CQDs: (Kanungo,2023) (Shabbir, 2021)

A 0.7 M citric acid solution was prepared in distilled water and microwaved at medium-high power in 3-minute intervals until a viscous, tar-like product formed. After cooling to room temperature, 20 mL distilled water was added and stirred to form a CQD solution. The solution underwent vacuum filtration, yielding a clear or slightly colored CQD solution.

5.1.2 Creation of the activated carbon (Thamer, 2023)

Moringa oleifera seeds were washed with deionized water and air-dried for 24 hours. The dried material was carbonized in a kiln at 600 °C for 1 hour. The resulting char was soaked in a 10% K_3PO_4 solution for chemical activation. After activation, the material was rinsed with distilled

water until a neutral pH was achieved. The activated carbon was subsequently ground and sieved to obtain particles between 0.150 mm and 0.425 mm in size.

5.1.3 Addition of graphene oxide nanoparticles:(Liu, 2023)

Graphene oxide nanoparticles (5 g) were dispersed in 10 mL of deionized water and added to the hydrogel precursor mixture at a 1:10 ratio (nanoparticle suspension to hydrogel) and thoroughly mixed.

5.1.4 Addition of the ethylene glycol(porogenic solvent): (Xu, 2023)

Ethylene glycol (EG) was added to the hydrogel precursor mixture at a 1:10 ratio.

5.1.5 Carboxyl group activation(Tian, 2019)

Hydrogels were treated with 5% hydrogen peroxide on an orbital shaker (50 rpm) for 5 hours, followed by UV-C exposure at a 6 cm distance for 24 hours. The hydrogel was rinsed with deionized water until neutral pH. After, the hydrogel soaked in 10% citric acid at 50 °C for 12 hours and was washed thoroughly with distilled water to remove residual ethylene glycol and citric acid.

6. Phase 5: Additive results and discussion

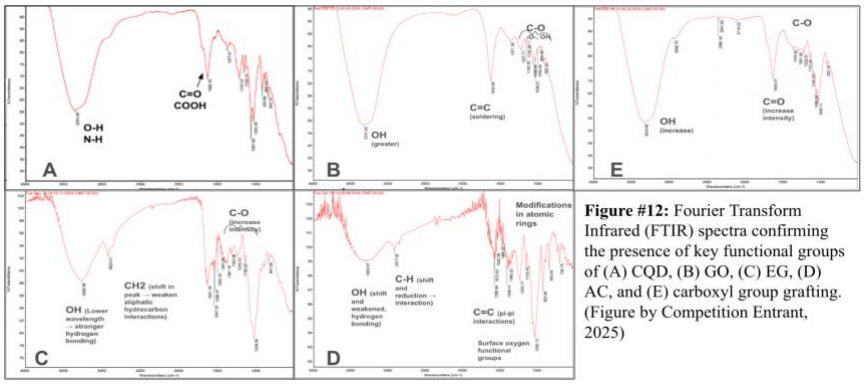

Figure #12: Fourier Transform Infrared (FTIR) spectra confirming the presence of key functional groups of (A) CQD, (B) GO, (C) EG, (D) AC, and (E) carboxyl group grafting. (Figure by Competition Entrant, 2025)

FTIR spectroscopy was used to confirm the successful incorporation and chemical functionality additives (Figure 12). Each spectrum revealed key functional groups contributing to interactions within the hydrogel matrix. In Figure 12A, CQD shows broad –OH/–NH stretching (~3300 cm^{-1}) and carboxylic C=O (~1700 cm^{-1}), indicating strong hydrogen bonding and electrostatic potential. GO (B) exhibits enhanced –OH, C=C, and C=O peaks, confirming aromatic and oxidized domains for π–π stacking and electrostatic dye binding. EG (C) shows weakened CH_2 and shifted –OH peaks, suggesting hydrogen bonding and altered swelling behavior. AC (D) displays broad –OH bands and reduced C–H/C=C intensities, reflecting surface oxidation that enhances van der Waals and electrostatic interactions. Lastly, carboxyl modification (E) is confirmed by intensified C=O, C–O, and –OH peaks, indicating improved polarity and crosslinking potential for enhanced dye adsorption.

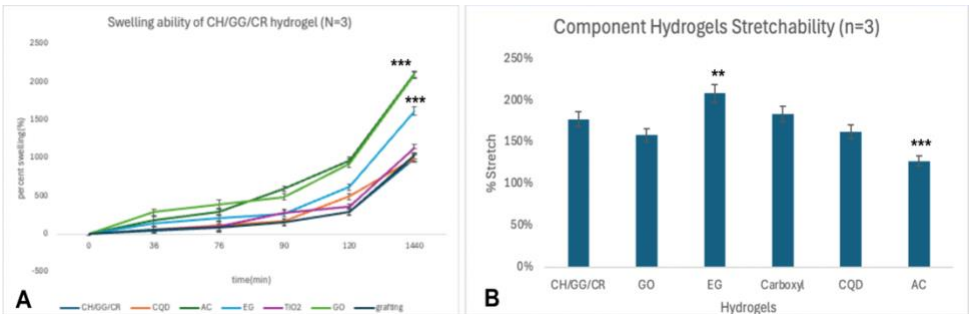

Figure #13: Evaluation of the physical effects of various additives on (A) Swelling behavior and (B) stretchability of CH/GG/CR hydrogels (N=3). Data is the percent (± 1 SE). Statistical significance was determined using Anova: Two-Factor With Replication with a post-hoc Tukey Test(*p < 0.05, **p < 0.01, ***p < 0.005 compared to CH/GG/CR)

The swelling and stretchability performance of CH/GG/CR hydrogels modified with various functional additives is shown in Figure #13. The swelling analysis (FIgure 13A) revealed that the incorporation of activated carbon (AC), graphene oxide (GO), and ethylene glycol (EG) significantly increased the hydrogel's swelling capacity compared to the unmodified CH/GG/CR formulation. The GO and carboxyl group grafted hydrogel reached over 2000% swelling after 1440 minutes (***p<0.005). The enhancement is from the activated carbon is most likely due to the heat induces dehydration and K3PO4 oxidation reactions with hydroxyl and carboxyl groups, generating CO_2 and water and forming a porous carbon matrix with a high surface area due to the etching and expansion of the carbon framework. Graphene oxide (GO) consists of loosely stacked 2D carbon sheets with high surface area and interlayer spacing, which allows water to diffuse more easily through the hydrogel and expand its network. Its abundant oxygen-containing functional groups (–OH, –COOH, –O–) form hydrogen bonds with water, significantly enhancing the hydrogel's hydrophilicity and swelling capacity. The stretchability results showed that the EG significantly increased the hydrogel extensibility (**p<0.01) likely acted as a plasticizer. The AC modified hydrogel exhibited the lowest stretchability (***p<0.005) which is due to the rigid structure of AC which reinforces the filler.

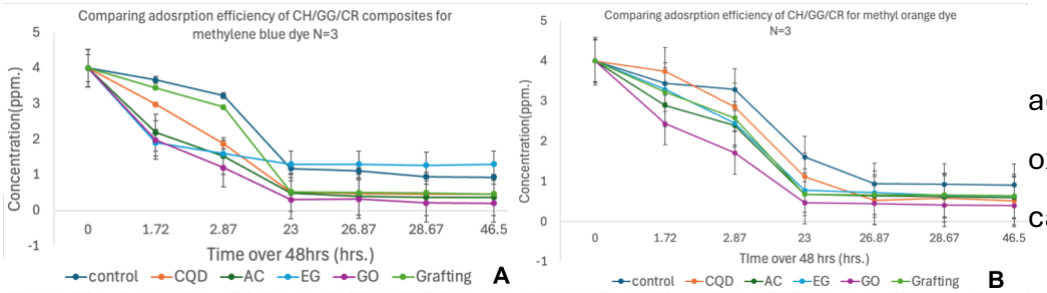

Figure #14: Adsorption efficiency of CH/GG/CR hydrogels modified with various additives over 48 hours for (A) MB (B) MO dyes (N=3). Dye concentration (ppm) was measured at multiple time points, with lower final concentrations indicating greater dye removal. Data is the percent (± 1 SE). Statistical significance was determined using Anova: Two-Factor With Replication with a post-hoc Tukey Test(*p < 0.05, **p < 0.01, ***p < 0.005 compared to CH/GG/CR)

Among all additives, graphene oxide (GO), activated carbon (AC), and carbon quantum dots (CQDs) showed the highest dye removal efficiency, with GO and AC reducing concentrations nearly to zero (***p < 0.005). GO's

extended π-conjugated domains enabled strong π–π stacking with aromatic dyes, while its –COOH, –OH, and –O– groups facilitated hydrogen bonding and electrostatic interactions. AC's sp^2-hybridized polyaromatic structure and oxygenated surface groups supported multiple binding modes, aided by its microporous–mesoporous architecture. CQDs, with sp^2/sp^3 hybridization and oxygen/nitrogen-rich surfaces, enabled efficient adsorption via hydrogen bonding, electrostatics, and π–π interactions. Ethylene glycol-modified hydrogels showed limited MO^- and moderate MB^+ removal, likely due to active site blockage.

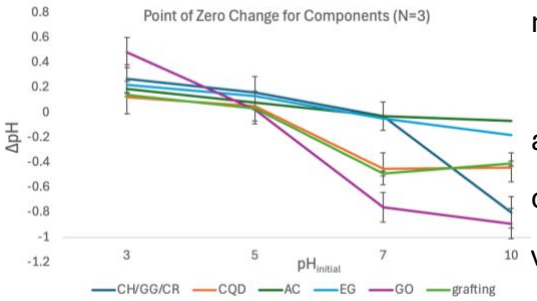

Figure #15: Point of Zero Change (PZC) of the additional hydrogel formulations (N=3), showing the relationship between initial pH and ΔpH after equilibration. The PZC values were determined by identifying the pH at which ΔpH = 0.

The unmodified CH/GG/CR hydrogel exhibited a PZC at approximately pH 6.68, while activated carbon (AC) and carbon quantum dots (CQD) showed slightly lower PZC values at 6.45 and 5.2, respectively, indicating differing surface charge behaviors.

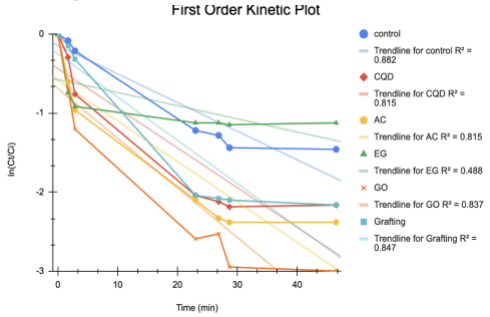

Figure #16: Pseudo-first order kinetic plot for dye adsorption onto unmodified and modified hydrogel samples (CQD, AC, EG, GO, and grafting). The plot shows $\ln(C_t/C_0)$ versus time (min), with trendlines fitted to determine the rate constant (k) and correlation coefficient (R^2) for each sample. Higher k values indicate faster adsorption rates, suggesting greater hydrogel efficiency. The R^2 values reflect the goodness-of-fit to the pseudo-first-order model, supporting a physisorption mechanism for most samples.

Figure #16 shows the pseudo-first-order kinetic plot for dye adsorption onto various hydrogel formulations, where $\ln(C_t/C_0)$ is plotted against time. This model assumes adsorption is proportional to available sites, indicating a physisorption mechanism driven by weak interactions such as van der Waals forces and hydrogen bonding. GO-modified hydrogels exhibited the highest k value(slope), indicating the fastest adsorption due to their high surface area and π–π interactions. CQD- and AC-modified hydrogels also showed rapid kinetics and good model fit (R^2 ≈ 0.815), due to their functionalized surfaces and high porosity. In contrast, EG-modified hydrogels showed the lowest k, likely due to site blockage. Overall, GO, CQDs, and AC significantly improved dye adsorption efficiency.

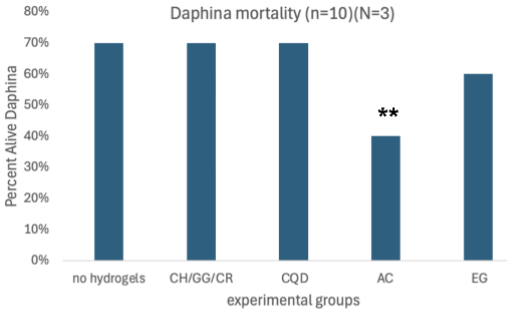

Figure #17: Biotoxicity assessment of hydrogel samples based on *Daphnia magna* mortality rate (n=10 per group)(N=3 trials). The percentage of live Daphnia magna was recorded after exposure to treated water from varying experimental groups. Statistical significance was determined using Anova: Two-Factor With Replication with a post-hoc Tukey Test(**p<0.01 compared to no hydrogels) (Figure by Competition Entrant, 2025)

The unmodified CH/GG/CR hydrogel, as well

as the CQD and EG-modified variants, showed high survival rates (approximately 70%), comparable to the no-hydrogel control, indicating low toxicity and good biocompatibility. Acceptable survival rates will be ones that are not significantly different from the control. In contrast, the AC-modified hydrogel resulted in a significantly lower survival rate of around 40% ($p < 0.01$), suggesting that the activated carbon may have introduced harmful residues that were detrimental to aquatic life.

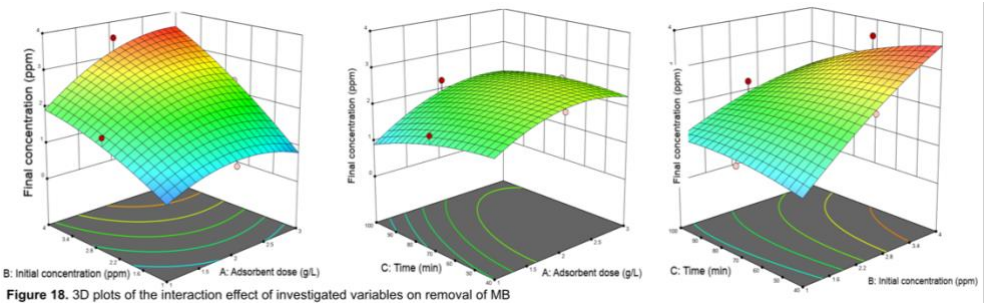

Figure 18. 3D plots of the interaction effect of investigated variables on removal of MB

Central composite design testing showed a successful quadratic model with a r^2 of 0.9. ANOVA tests showed successful modeling with a p-value of 0.0014 being significant and a lack of fit p-value of 0.27 being not significant. Optimized values of adsorbent dose, initial concentration and contact time resulted to be 3 g/mL, 1ppm, and 40min respectively.

7. Phase 6: Apparatus Testing

7.1 3D Printed Column

A column was designed on Onshape with three fan-shaped sections. The dimensions were 12 cm in length and 0.98 cm in width, with square-shaped gaps measuring 1.5 mm by 1.5 mm. The column was designed to be 0.3 mm thick. The design was sliced using Bambu Studio and printed using a Bambu A1.

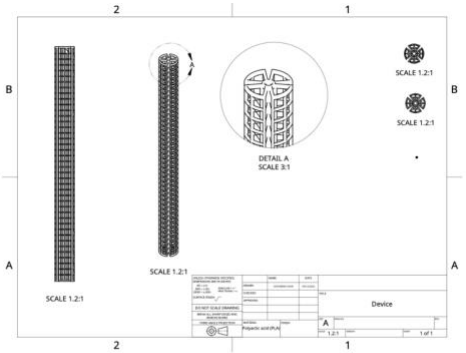

Figure #18: Structural details of the 3D-printed device, including an isometric view (left) and a detailed view (right) of the top section, highlighting the internal configuration. The device is printed using Polylactic acid (PLA) and is scaled at 1.2:1, with a magnified detail view at 3:1.

Parameters			
mass of hydrogel	volume of dye	length of tube	ID tube
0.56g	3000mL	750cm	1/8 in
Measurements			
Motor speed	Flow Rate	Residence Time	# of cycles
31	28.8mL/min	25 seconds	5
Optimizaitons			
Time for MB	Time for HCl	Time for MO	Time for NaOH
48 min	1min 18 seconds	53 min	58 seconds
Volume for MB	Volume for HCl	Volume for MO	Volume for NaOH
1382.4mL	37.44mL	1526.4mL	27.84mL
Amount for MB	Amount for HCl	Amount for MO	Amount for NaOH
5.53mg	3.74mmol	5.31mg	2.78mmol
Efficiency			
Adsorption	Desproption	Cumulative	Hydrogel retention
0.47ppm	10.2ppm	26.91mg	7.26mL
Adsorption	Desproption	Cumulative	Hydrogel retention
0.56ppm	9.8ppm	19.9mg	7.18mL

Figure #19: Operational parameters, optimization data, and efficiency metric for auto cleaning hydrogel-based dye remediation system.

7.2 Apparatus Setup

Hydrogels were minced and inserted into the 3D printed apparatus. The hydrogel-filled apparatus was inserted into a Kimble Flex column (12 mL total, 15 cm length, 1 cm ID). A peristaltic pump fed the initial dye solution through the tubing (Fisher Scientific, 13-876-3) set at an optimized motor speed and passed through the tubing/inserted column. Effluent was collected in a separate flask.

7.3 Auto Cleaning

To enable auto-cleaning, a DROK timer relay was connected to a 1.8” solenoid valve with a 2-position, 5-way junction box to alternate between dye and cleaning solutions at optimized intervals. A peristaltic pump set to an optimized speed drove the solution through the column. The solenoid valve-timer relay setup directed the treated cleaning solution for reuse and recirculated the dye solution back to the original container.

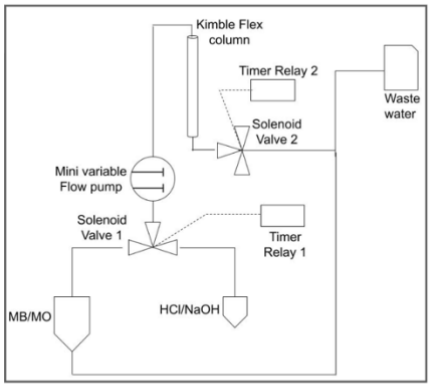

Figure 20: Schematic flow chart of auto cleaning process

7.4 Optimization

Motor speed was optimized as the minimum rate allowing continuous flow through the apparatus (30). Dye solution timing and volume were determined by sampling every 10 minutes until concentration stabilized, indicating hydrogel saturation. Cleaning solution timing was determined by sampling every 20 seconds until dye levels neared 0 ppm, confirming complete desorption. This process was repeated each cycle until dye concentrations plateaued. Figure 19 summarizes the setup, optimization, and performance. A total of 0.56 g of hydrogel treated 3000 mL of dye solution, achieving adsorption capacities of 0.47 ppm for MB and 0.56 ppm for MO, with desorption values of 10.2 ppm and 9.8 ppm, respectively. The hydrogel showed high cumulative adsorption (26.91 mg) and consistent retention capacity (7.2 mL), confirming its reusability and suitability for continuous remediation.

8. Conclusion

In conclusion, this study presents a biocompatible and sustainable hydrogel-based approach to dye remediation, using a 1:1:1 blend of chitosan, gellan gum, and κ-carrageenan. The alternate hypothesis was supported. Among the modified variants, hydrogels enhanced with graphene oxide, activated carbon, and carbon quantum dots (CQDs) showed the highest adsorption, with CQDs offering superior biocompatibility and cost-efficiency due to their in-lab synthesis from citric acid. The hydrogels demonstrated strong reusability, with NaOH and HCl enabling effective desorption of methyl orange and methylene blue, respectively, where in a wastewater facility two separate treatment systems will be needed. Integration with a 3D-printed auto-cleaning system enabled programmable, low-maintenance operation with minimal

environmental impact. This system offers a scalable and eco-friendly solution for continuous wastewater treatment, combining natural materials with smart engineering.

9. Future Studies

While the hydrogel-based dye remediation showed strong performance, several limitations remain such as real world implantation and scalability to handle large amounts of realistic wastewater. Real wastewater conditions with mixed contaminants could not be tested due to budget constraints, and hazardous dyes were excluded for safety reasons. Plant-based hydrogel synthesis was also limited by equipment and cost. Future studies should address these challenges and explore scaling the auto-cleaning system for industrial use.

I. Bibliography

Ahmed, E. M. (2015). Hydrogel: Preparation, characterization, and applications: A review. Journal of Advanced Research, 6(2), 105–121. https://doi.org/10.1016/j.jare.2013.07.006

Al-Tohamy, Rania, et al. "A Critical Review on the Treatment of Dye-Containing Wastewater: Ecotoxicological and Health Concerns of Textile Dyes and Possible Remediation Approaches for Environmental Safety." Ecotoxicology and Environmental Safety, vol. 231, no. 0147-6513, Feb. 2022, p. 113160, www.sciencedirect.com/science/article/pii/S0147651321012720, https://doi.org/10.1016/j.ecoenv.2021.113160.

Team, A. (2022, May 23). *Drawing molecules*. Avogadro. https://avogadro.cc/docs/getting-started/drawing-molecules/

Bahrodin, M.B., Zaidi, N.S., Hussein, N. *et al*. Recent Advances on Coagulation-Based Treatment of Wastewater: Transition from Chemical to Natural Coagulant. *Curr Pollution Rep* **7**, 379–391 (2021). https://doi.org/10.1007/s40726-021-00191-7

Cano-Vincent, A., Tuñón-Molina, A., Bakshi, H., Serra, R. S. I., Alfagih, I. M., Tambuwala, M. M., & Serrano-Aroca, Á. (2023). Biocompatible Alginate Film Crosslinked with Ca2+ and Zn2+ Possesses Antibacterial, Antiviral, and Anticancer Activities. *ACS Omega*, *8*(27), 24396–24405. https://doi.org/10.1021/acsomega.3c01935

Dhahir, S. A., Braihi, A. J., & Habeeb, S. A. (2024). Comparative Analysis of Hydrogel Adsorption/Desorption with and without Surfactants. *Gels*, *10*(4), 251. https://doi.org/10.3390/gels10040251

Getya, D., Lucas, A., & Gitsov, I. (2023). Composite hydrogels based on Poly(Ethylene glycol) and cellulose macromonomers as fortified materials for environmental cleanup and clean water safeguarding. *International Journal of Molecular Sciences*, *24*(8), 7558. https://doi.org/10.3390/ijms24087558

Guo, H., Jiao, T., Zhang, Q., Guo, W., Peng, Q., & Yan, X. (2015). Preparation of graphene Oxide-Based hydrogels as efficient dye adsorbents for wastewater treatment. *Nanoscale Research Letters*, *10*(1). https://doi.org/10.1186/s11671-015-0931-2

Kanungo, S., Gupta, N., Rawat, R., Jain, B., Solanki, A., Panday, A., Das, P., & Ganguly, S. (2023b). Doped carbon quantum dots reinforced hydrogels for sustained delivery of molecular cargo. Journal of Functional Biomaterials, 14(3), 166. https:// doi.org/10.3390/jfb14030166

Kjidaa, B., Mchich, Z., Aziz, K., Saffaj, N., Saffaj, T., & Mamouni, R. (2024). Flexible synthesis of io-Hydroxyapatite/ Chitosan hydrogel beads for highly efficient orange G dye removal: Batch and Recirculating Fixed-Bed Column study. ACS Omega. https://doi.org/10.1021/acsomega.3c10054

Liu, M., Wang, Y., Wu, Y., Liu, C., & Liu, X. (2023). Preparation of Graphene Oxide Hydrogels and Their Adsorption Applications toward Various Heavy Metal Ions in Aqueous Media. *Applied Sciences*, *13*(21), 11948. https://doi.org/10.3390/app132111948

Luftman, M. (2018, December 19). Introduction to UV/VIS spectrophotometry: using spectrophotometer to determine concentration. PROAnalytics, LLC. https://pro-analytics.net/using-spectrophotometer-to-determine-concentration/

Makrygianni, M., Christofili, A., & Deimede, V. (2021). Emulsion-templated macroporous ammonium based polymers: Synthesis and dye adsorption study. *Colloids and Surfaces a Physicochemical and Engineering Aspects*, *610*, 125634. https://doi.org/10.1016/j.colsurfa.2020.125634

Mohamed, M., Jaafar, J., Ismail, A., Othman, M., & Rahman, M. (2017). Fourier Transform Infrared (FTIR) spectroscopy. In *Elsevier eBooks* (pp. 3–29). https://doi.org/10.1016/b978-0-444-63776-5.00001-2

Neese, F. Software update: the ORCA program system -- Version 5.0 Wiley Interdiscip. Rev.: Comput. Mol. Sci., 2022, 12, 1, e1606 (DOI: 10.1002/wcms.1606)

Reddy, P. R. S., Rao, K. M., Rao, K. S. V. K., Shchipunov, Y., & Ha, C. (2014). Synthesis of alginate based silver nanocomposite hydrogels for biomedical applications. *Macromolecular Research*, *22*(8), 832–842. https://doi.org/10.1007/s13233-014-2117-7

Reilly, K., Ellis, L. A., Davoudi, H. H., Supian, S., Maia, M. T., Silva, G. H., Guo, Z., Martinez, D. S. T., & Lynch, I. (2023). Daphnia as a model organism to probe biological responses to nanomaterials—from individual to population effects via adverse outcome pathways. Frontiers in Toxicology, 5. https://doi.org/10.3389/ftox.2023.1178482

Shabbir, H., Tokarski, T., Ungor, D., & Wojnicki, M. (2021). Eco friendly synthesis of carbon dot by hydrothermal method for metal ions salt identification. Materials, 14(24), 7604. https://doi.org/10.3390/ma14247604

Srivastava, N., & Choudhury, A. R. (2021). Green synthesis of PH-Responsive, Self-Assembled, novel polysaccharide composite hydrogel and its application in selective capture of Cationic/Anionic dyes. Frontiers in Chemistry, 9. https://doi.org/10.3389/fchem.2021.761682

Tian, Y., Liang, G., Fan, T., Shang, J., Shang, S., Ma, Y., Matsuda, R., Liu, M., Wang, M., Li, L., & Kitagawa, S. (2019). Grafting Free Carboxylic Acid Groups onto the Pore Surface of 3D Porous Coordination Polymers for High Proton Conductivity. *Chemistry of Materials*, *31*(20), 8494–8503. https://doi.org/10.1021/acs.chemmater.9b02924

Thamer, B. M., Al-Aizari, F. A., & Abdo, H. S. (2023). Activated Carbon-Incorporated Tragacanth Gum Hydrogel Biocomposite: A Promising Adsorbent for Crystal Violet Dye Removal from Aqueous Solutions. Gels, 9(12), 959. https://doi.org/10.3390/gels9120959

Wamba, A. G., Kofa, G. P., Koungou, S. N., Thue, P. S., Lima, E. C., Reis, G. S. D., & Kayem, J. G. (2018). Grafting of Amine functional group on silicate based material as adsorbent for water purification: A short review. *Journal of Environmental Chemical Engineering*, *6*(2), 3192–3203. https://doi.org/10.1016/j.jece.2018.04.062

Xu, X., Guillomaitre, N., Christie, K. S. S., Bay, R. K., Bismarck, N., Datta, S. S., Ren, Z. J., & Priestley, R. D. (2023). Quick-Release antifouling hydrogels for Solar-Driven water purification. ACS Central Science, 9(2), 177–185. https://doi.org/10.1021/acscentsci.2c01245